

May 2001  
hep-ph/0106020

# Electroweak radiative corrections: Towards a full two-loop analysis

ADRIAN GHINCULOV<sup>a\*</sup> AND YORK-PENG YAO<sup>b†</sup>

<sup>a</sup>*Department of Physics and Astronomy, UCLA,  
Los Angeles, California 90095-1547, USA*

<sup>b</sup>*Randall Laboratory of Physics, University of Michigan,  
Ann Arbor, Michigan 48109-1120, USA*

In calculating electroweak radiative corrections at two-loop level, one encounters Feynman graphs with several different masses on the internal propagators and on the external legs, which lead to complicated scalar functions. We describe a general analytic-numerical reduction scheme for evaluating any two-loop diagrams with general kinematics and general renormalizable interactions, whereby ten basic functions form a complete set after tensor reduction. We illustrate this scheme by applying it to two- and three-point functions. We discuss the treatment of infrared singularities within this numerical approach.

Presented at the

5th International Symposium on Radiative Corrections  
(RADCOR-2000)

Carmel CA, USA, 11–15 September, 2000

---

<sup>\*</sup>Work supported by the US Department of Energy.

<sup>†</sup>Work supported by the US Department of Energy.

Because of the level of experimental precision attained in measuring the electroweak parameters at LEP, SLC, and Tevatron, a full two-loop analysis is desirable. This will be even more necessary in view of the precision envisioned at future colliders such as the LHC, NLC, and the GigaZ.

While several two-loop quantities are already included in standard electroweak fitting programs such as ZFITTER [1], they are often obtained within certain approximations where one can neglect certain masses or can perform a mass expansion of Feynman graphs. These approximation techniques, while ingenious, were used because the exact Feynman integrals typically lead to complicated scalar functions which often cannot be evaluated analytically, in a closed form, in terms of usual special functions. During the past decade, the existing work on massless [2] and massive [3]–[11] two-loop graphs made it clear that for the general mass case, a certain amount of numerical work is unavoidable.

Here we discuss the status of a hybrid, analytical-numerical approach to two-loop radiative corrections with arbitrary masses. The aim is to treat any two-loop graph, of any topology, by using the same algorithm, so that the general recipe can be encoded in a computer program. Such an approach was developed in ref. [5], and was successfully applied to several physical processes [6]–[8].

At the center of this approach is the introduction of a set of ten basic functions,  $h_1$ — $h_{10}$ , defined by the following one-dimensional integral representations:

$$\begin{aligned}
h_1(m_1, m_2, m_3; k^2) &= \int_0^1 dx \tilde{g}(x) \\
h_2(m_1, m_2, m_3; k^2) &= \int_0^1 dx [\tilde{g}(x) + \tilde{f}_1(x)] \\
h_3(m_1, m_2, m_3; k^2) &= \int_0^1 dx [\tilde{g}(x) + \tilde{f}_1(x)] (1-x) \\
h_4(m_1, m_2, m_3; k^2) &= \int_0^1 dx [\tilde{g}(x) + \tilde{f}_1(x) + \tilde{f}_2(x)] \\
h_5(m_1, m_2, m_3; k^2) &= \int_0^1 dx [\tilde{g}(x) + \tilde{f}_1(x) + \tilde{f}_2(x)] (1-x) \\
h_6(m_1, m_2, m_3; k^2) &= \int_0^1 dx [\tilde{g}(x) + \tilde{f}_1(x) + \tilde{f}_2(x)] (1-x)^2 \\
h_7(m_1, m_2, m_3; k^2) &= \int_0^1 dx [\tilde{g}(x) + \tilde{f}_1(x) + \tilde{f}_2(x) + \tilde{f}_3(x)] \\
h_8(m_1, m_2, m_3; k^2) &= \int_0^1 dx [\tilde{g}(x) + \tilde{f}_1(x) + \tilde{f}_2(x) + \tilde{f}_3(x)] (1-x) \\
h_9(m_1, m_2, m_3; k^2) &= \int_0^1 dx [\tilde{g}(x) + \tilde{f}_1(x) + \tilde{f}_2(x) + \tilde{f}_3(x)] (1-x)^2 \\
h_{10}(m_1, m_2, m_3; k^2) &= \int_0^1 dx [\tilde{g}(x) + \tilde{f}_1(x) + \tilde{f}_2(x) + \tilde{f}_3(x)] (1-x)^3, \quad (1)
\end{aligned}$$

where:

$$\begin{aligned}
\tilde{g}(m_1, m_2, m_3; k^2; x) &= Sp\left(\frac{1}{1-y_1}\right) + Sp\left(\frac{1}{1-y_2}\right) + y_1 \log \frac{y_1}{y_1-1} + y_2 \log \frac{y_2}{y_2-1} \\
\tilde{f}_1(m_1, m_2, m_3; k^2; x) &= \frac{1}{2} \left[ -\frac{1-\mu^2}{\kappa^2} + y_1^2 \log \frac{y_1}{y_1-1} + y_2^2 \log \frac{y_2}{y_2-1} \right] \\
\tilde{f}_2(m_1, m_2, m_3; k^2; x) &= \frac{1}{3} \left[ -\frac{2}{\kappa^2} - \frac{1-\mu^2}{2\kappa^2} - \left( \frac{1-\mu^2}{\kappa^2} \right)^2 \right. \\
&\quad \left. + y_1^3 \log \frac{y_1}{y_1-1} + y_2^3 \log \frac{y_2}{y_2-1} \right] \\
\tilde{f}_3(m_1, m_2, m_3; k^2; x) &= \frac{1}{4} \left[ -\frac{4}{\kappa^2} - \left( \frac{1}{3} + \frac{3}{\kappa^2} \right) \left( \frac{1-\mu^2}{\kappa^2} \right) - \frac{1}{2} \left( \frac{1-\mu^2}{\kappa^2} \right)^2 - \left( \frac{1-\mu^2}{\kappa^2} \right)^3 \right. \\
&\quad \left. + y_1^4 \log \frac{y_1}{y_1-1} + y_2^4 \log \frac{y_2}{y_2-1} \right] . \quad (2)
\end{aligned}$$

Here we use the following notations:

$$\begin{aligned}
y_{1,2} &= \frac{1 + \kappa^2 - \mu^2 \pm \sqrt{\Delta}}{2\kappa^2} \\
\Delta &= (1 + \kappa^2 - \mu^2)^2 + 4\kappa^2\mu^2 - 4i\kappa^2\eta , \quad (3)
\end{aligned}$$

and

$$\begin{aligned}
\mu^2 &= \frac{ax + b(1-x)}{x(1-x)} \\
a &= \frac{m_2^2}{m_1^2}, \quad b = \frac{m_3^2}{m_1^2}, \quad \kappa^2 = \frac{k^2}{m_1^2} . \quad (4)
\end{aligned}$$

The evaluation of these ten functions is best done by numerical integration. By using an adaptative deterministic numerical integration algorithm, these one-dimensional integrals can be calculated fast and very precisely. By numerical integration, we plot these ten basic functions in figure 1 for a range of their kinematic variables.

Within the method we discuss here, any two-loop diagram with arbitrary masses is first reduced to multi-dimensional scalar integrals involving these ten basic functions  $h_i$ . In ref. [5] we have shown that this can always be done for any two-loop diagrams occuring in renormalizable theories. We note in passing that for the case of non-renormalizable theories this set of ten functions  $h_i$  in general needs to be extended to include additional functions.

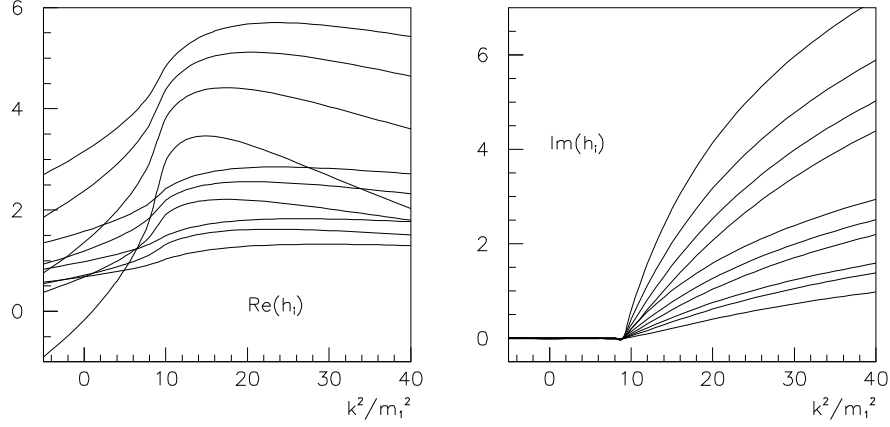


Figure 1: Plots of the ten basic functions  $h_i(m_1^2, m_2^2, m_3^2; -k^2)$  as a function of the external momentum variable  $k^2$ . The plots given here are for  $m_1^2 = m_2^2 = m_3^2 = 1$ .

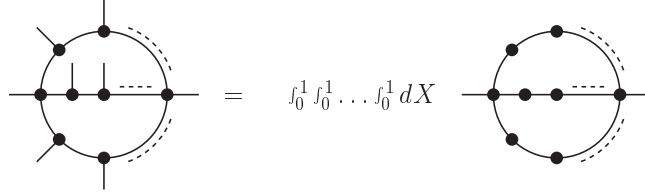


Figure 2: Expressing generic massive two-loop Feynman diagrams as integrals over sunset-type functions.

This reduction procedure starts by introducing Feynman parameters in the original Feynman graph in order to relate the integral to sunset-type integrals. This is illustrated in figure 2.

At this point, the Feynman graph is written as a multi-dimensional integral over tensor integrals of the following type:

$$\int d^n p d^n q \frac{p^{\mu_1} \dots p^{\mu_i} q^{\mu_{i+1}} \dots q^{\mu_j}}{[(p+k)^2 + m_1^2]^{\alpha_1} (q^2 + m_2^2)^{\alpha_2} (r^2 + m_3^2)^{\alpha_3}} \quad (5)$$

In the following step, these tensor integrals are decomposed into scalar integrals, whereby the Lorentz structure is constructed from the vector  $k^\mu$  and the metric tensor  $g^{\mu\nu}$ . This can be carried out systematically by decomposing the loop momenta  $p$  and  $q$  into components parallel and orthogonal to  $k^\mu$ . For instance, the decomposition of all tensor integrals up to rank three is the following:

$$\begin{aligned}
\frac{1}{[211]} &= {}_1A_1, \quad \frac{p^\mu}{[211]} = k^\mu {}_2A_1, \quad \frac{q^\mu}{[211]} = k^\mu {}_3A_1 \\
\frac{p^\mu p^\nu}{[211]} &= \tau^{\mu\nu} {}_4A_1 + g^{\mu\nu} {}_4A_2, \quad \frac{p^\mu q^\nu}{[211]} = \tau^{\mu\nu} {}_5A_1 + g^{\mu\nu} {}_5A_2, \quad \frac{q^\mu q^\nu}{[211]} = \tau^{\mu\nu} {}_6A_1 + g^{\mu\nu} {}_6A_2 \\
\frac{p^\mu p^\nu p^\lambda}{[211]} &= (\tau^{\mu\nu} k^\lambda + \tau^{\mu\lambda} k^\nu + \tau^{\nu\lambda} k^\mu) {}_7A_1 + (g^{\mu\nu} k^\lambda + g^{\mu\lambda} k^\nu + g^{\nu\lambda} k^\mu) {}_7A_2 \\
\frac{q^\mu p^\nu p^\lambda}{[211]} &= (\tau^{\mu\nu} k^\lambda + \tau^{\mu\lambda} k^\nu + \tau^{\nu\lambda} k^\mu) {}_8A_1 + (g^{\mu\nu} k^\lambda + g^{\mu\lambda} k^\nu + g^{\nu\lambda} k^\mu) {}_8A_2 \\
\frac{p^\mu q^\nu q^\lambda}{[211]} &= (\tau^{\mu\nu} k^\lambda + \tau^{\mu\lambda} k^\nu + \tau^{\nu\lambda} k^\mu) {}_9A_1 + (g^{\mu\nu} k^\lambda + g^{\mu\lambda} k^\nu + g^{\nu\lambda} k^\mu) {}_9A_2 \\
&\quad + (g^{\mu\nu} k^\lambda + g^{\mu\lambda} k^\nu - 2g^{\nu\lambda} k^\mu) {}_9A_3 \\
\frac{q^\mu q^\nu q^\lambda}{[211]} &= (\tau^{\mu\nu} k^\lambda + \tau^{\mu\lambda} k^\nu + \tau^{\nu\lambda} k^\mu) {}_{10}A_1 + (g^{\mu\nu} k^\lambda + g^{\mu\lambda} k^\nu + g^{\nu\lambda} k^\mu) {}_{10}A_2
\end{aligned} \tag{6}$$

In the formulae above, a loop integration  $\int d^n p \, d^n q$  is understood, and we used the following notations:

$$[211] = [(p+k)^2 + m_1^2]^2 (q^2 + m_2^2) (r^2 + m_3^2) \quad , \quad \tau^{\mu\nu} = g^{\mu\nu} - \frac{k^\mu k^\nu}{k^2} \tag{7}$$

In ref. [5] we have shown that all the scalar coefficients  ${}_iA_j$  involved in this tensor decomposition are directly expressible in terms of the ten basic functions  $h_i$ , up to trivial one-loop tadpole integrals. In all the formulae above, we have considered only integrals with a special combination of propagator powers, namely [211] of eq. 6. Where integrals with higher powers are needed, they can be obtained directly by mass differentiation. The only two-loop combination with lower power, [111], can be obtained from [211] by a recursion formula obtained by partial integration [5].

After performing these steps, the Feynman graph is decomposed into scalar integrals expressed essentially as multiple integrals over  $h_i$  functions, plus trivial one-loop tadpole-type contributions. All necessary formulae to perform this reduction are given in ref. [5]. They were encoded into computer algebra programs for automatizing the reduction.

Once this standard integral representation is obtained for all Feynman graphs involved in a physical process, the final step consists in a numerical multi-dimensional integration of these expressions. The numerical integration uses an adaptative deterministic algorithm, similar to the numerical integration for the  $h_i$  functions. This ensures an efficient and precise evaluation of the integrals.

Several physical calculations have been performed so far by using this method. As a two-point example to test the reduction algorithm and the reliability of the numerical integration, in figure 3 we show the mixed electroweak-QCD Feynman

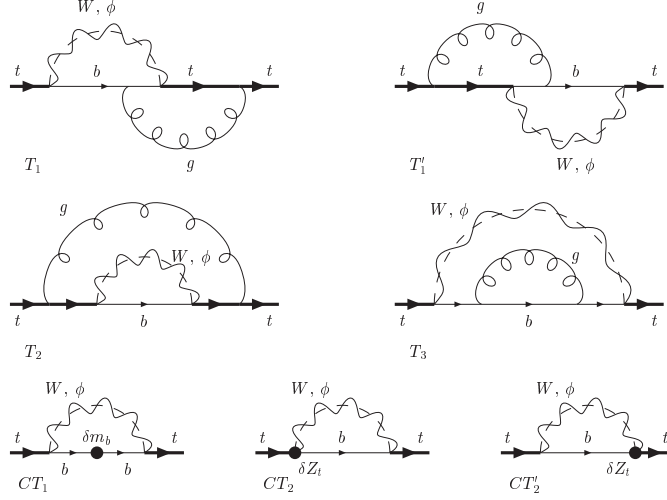


Figure 3: The two-loop Feynman graphs which contribute to the  $b$ -mass dependent correction of  $\mathcal{O}(\alpha_s g^2)$  to the top self-energy. Only the counterterm diagrams are shown which are needed for subtracting the infinities of the imaginary part of the self-energy, which gives the  $\mathcal{O}(\alpha_s)$  correction to the  $t \rightarrow W + b$  decay.

$m_t$ [GeV]	160	165	170	175	180
$\Gamma_t^{tree}$ [GeV]	1.127	1.260	1.402	1.553	1.712
$\delta\Gamma_t^{1-loop}$ [GeV]	-.092	-.104	-.117	-.132	-.149

Table 1: The  $\mathcal{O}(\alpha_s)$  correction to the top decay  $t \rightarrow W + b$  as obtained from the imaginary part of the two-loop top self-energy of figure 1, integrated numerically. We took  $G_F = 1.16637 \cdot 10^{-5} \text{ GeV}^{-2}$ ,  $m_W = 80.41 \text{ GeV}$ ,  $m_b = 4.7 \text{ GeV}$ , and  $\alpha_s(m_t) = .108$ .

graphs which contribute to the top quark self-energy at two-loop. By calculating the self-energy function  $\Sigma(p \cdot \gamma) = \Sigma_1(p \cdot \gamma) + \gamma_5 \cdot \Sigma_{\gamma_5}(p \cdot \gamma)$  at two-loop, from its imaginary part one can extract the top decay width up to  $\mathcal{O}(\alpha_s)$ , as  $\Gamma_t = 2 \cdot \text{Im}\Sigma_1(p \cdot \gamma = m_t)$ . Since this correction is known in an analytic form, this provides a good check on our two-loop algorithm. The results for the correction to the width, obtained from the imaginary part of the two-loop self-energy, are given in table 1. They agree with the existing analytic results.

As a three-point example, in figure 4 we show the diagrams which contribute to the top-dependent decay process  $Z \rightarrow b\bar{b}$ .

A point which deserves special attention in this case is the presence of IR divergences. Because the general formulae of the  $h_i$  functions are derived for general, finite masses, IR divergences in our method are not automatically extracted as poles in the space-time regulator, as is customary in QCD calculations. IR divergences

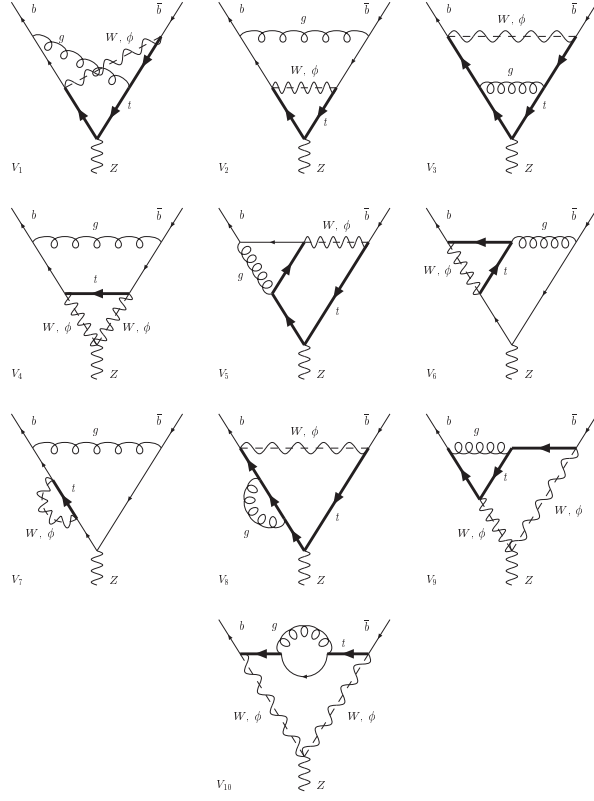


Figure 4: Two-loop three-point diagrams contributing to  $Z \rightarrow b\bar{b}$  at  $\mathcal{O}(\alpha_s g^2)$ .

in our approach usually appear as end-point singularities in the Feynman parameter integration over  $h_i$  functions, and therefore require a special treatment.

For both cases at hand – the top quark self-energy and the  $Z \rightarrow b\bar{b}$  decay – one possible approach is to use a mass regulator for the gluon. While in general this is not possible for non-abelian theories because it does not preserve the Slavnov-Taylor identities, in the particular case of these mixed electroweak-QCD corrections this is a correct procedure because at this order the IR structure is the same as in the abelian case.

Another approach is to extract the IR structure of the graphs analytically before numerical integration. This can be done in the form of one-loop integrals which can be handled separately in an analytical way, by usual dimensional regularization. This is illustrated in fig. 5. Once the IR divergences are extracted in the form of one-loop integrals, the two-loop integration can be carried out numerically.

We give in table 2 numerical results for all two-loop Feynman graphs involved in this process. The numerical results are after the extraction of the UV poles. The IR singularities are subtracted as shown in figure 5. The numerical integration accuracy

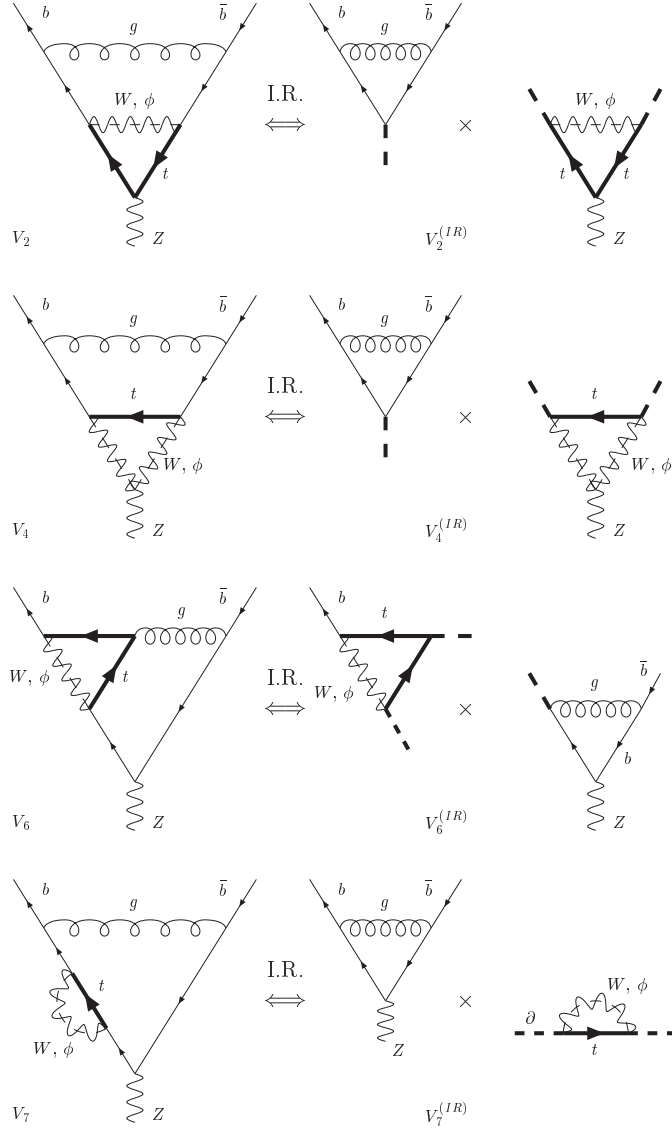


Figure 5: *Extracting the infrared divergent pieces of the two-loop diagrams analytically. The infrared divergency of the two-loop diagram is the same as the infrared divergency of the product of the two one-loop diagrams obtained by “freezing” the common line in the loop momenta integration.*



diagram	$m_t = 165 \text{ GeV}$	$m_t = 175 \text{ GeV}$	$m_t = 185 \text{ GeV}$
$V_1$	$-1.009 \cdot 10^{-3}$	$-7.187 \cdot 10^{-4}$	$-4.057 \cdot 10^{-4}$
$V_2 - V_2^{(IR)}$	$(-2.873 + i2.122) \cdot 10^{-3}$	$(-2.490 + i1.147) \cdot 10^{-3}$	$(-2.087 + i0.9274) \cdot 10^{-3}$
$V_3$	$1.545 \cdot 10^{-3}$	$2.255 \cdot 10^{-3}$	$3.034 \cdot 10^{-3}$
$V_4 - V_4^{(IR)}$	$(1.215 - i2.481) \cdot 10^{-2}$	$(1.242 - i2.570) \cdot 10^{-2}$	$(1.266 - i2.660) \cdot 10^{-2}$
$V_5$	$2.107 \cdot 10^{-2}$	$2.469 \cdot 10^{-2}$	$2.861 \cdot 10^{-2}$
$V_6 - V_6^{(IR)}$	$(3.089 - i4.257) \cdot 10^{-2}$	$(3.500 - i4.824) \cdot 10^{-2}$	$(3.950 - i5.445) \cdot 10^{-2}$
$V_7 - V_7^{(IR)}$	$(-0.7778 + i1.281) \cdot 10^{-2}$	$(-0.8001 + i1.349) \cdot 10^{-2}$	$(-0.8232 + i1.420) \cdot 10^{-2}$
$V_8$	$-1.059 \cdot 10^{-3}$	$-1.474 \cdot 10^{-3}$	$-1.942 \cdot 10^{-3}$
$V_9$	$6.289 \cdot 10^{-2}$	$6.703 \cdot 10^{-2}$	$7.143 \cdot 10^{-2}$
$V_{10}$	$-1.402 \cdot 10^{-2}$	$-1.389 \cdot 10^{-2}$	$-1.380 \cdot 10^{-2}$

Table 2: Numerical values for the two-loop diagrams shown in figure 4.  $V_1$ – $V_{10}$  are the sums of the corresponding  $W$  and  $\phi$  exchange graphs. An overall color and coupling constant factor of  $i\gamma_\mu(1-\gamma_5)\alpha_s(g^3/12\cos\theta_W)$  is understood. The UV and IR divergences are removed as discussed in the text.

is  $10^{-3}$ . The evaluation of a total of 78 Feynman graph evaluations with this precision required 100 hours computing time on a 600 MHz Pentium machine.

To conclude, we developed an algorithm for the tensor reduction of massive two-loop diagrams. It applies in principle to any massive two-loop graph, and it can be automatized in the form of a computer algebra program. The tensor decomposition algorithm results in a multi-dimensional integral over a set of ten basic functions  $h_i$ , which are defined in terms of one-dimensional integral representations. We described the numerical methods which we used for carrying out the remaining integrations.

We have shown how these techniques work in the case of two realistic calculations of mixed electroweak-QCD radiative corrections. The first example is the two-loop top quark self-energy from which the  $O(\alpha_s)$  correction to the top quark decay width can be extracted and compared with the analytical result. The second example is a three-point calculation involving all two-loop diagrams which contribute to the top-dependent decay process  $Z \rightarrow b\bar{b}$ . Thus we have shown that the techniques we described can be used in realistic calculations, where several internal mass and external momenta scales are involved.

This approach works for any such combination of kinematic variables, apart from possible infrared complications. In the context of the  $Z \rightarrow b\bar{b}$  example, we discussed the analytical separation of the infrared divergencies. Within our two-loop methods, if a process involves infrared singularities, these have to be dealt with in a special way because the numerical nature of our methods.

## References

- [1] D. Bardin, P. Christova, M. Jack, L. Kalinovskaya, A. Olchevski, S. Riemann, T. Riemann, *Comput. Phys. Commun.* **133** (2001) 229.
- [2] Z. Bern, L. Dixon, A. Ghinculov, *Phys. Rev.* **D63** (2001) 053007; C. Anastasiou, E.W.N. Glover, M.E. Tejeda-Yeomans, C. Oleari, *Nucl. Phys.* **0B601** (2001) 318; *Nucl. Phys.* **0B601** (2001) 341; *hep-ph/0011094*; *hep-ph/0010212*; E.W.N. Glover, C. Oleari, M.E. Tejeda-Yeomans, *hep-ph/0102201*; Z. Bern, L. Dixon, D.A. Kosower, *JHEP* **0001** (2000) 027; J.B. Tausk, *Phys. Lett.* **B469** (1999) 225; C. Anastasiou, T. Gehrmann, C. Oleari, E. Remiddi, J.B. Tausk, *hep-ph/0003261*; *Nucl. Phys.* **B580** (2000) 577; V.A. Smirnov, *Phys. Lett.* **B460** (1999) 397; V.A. Smirnov, O.L. Veretin, *Nucl. Phys.* **B566** (2000) 469; J.A.M. Vermaseren, S.A. Larin, T. van Ritbergen, *Phys. Lett.* **B405** (1997) 327; *Phys. Lett.* **B404** (1997) 153; *Phys. Lett.* **B400** (1997) 379.
- [3] G. Weiglein, R. Scharf, M. Böhm, *Nucl. Phys.* **B416** (1994) 606.
- [4] S. Bauberger and G. Weiglein, *Phys. Lett.* **B419** (1998) 333; *Nucl. Instrum. Meth.* **A389** (1997) 318.
- [5] A. Ghinculov and Y.-P. Yao, *Nucl. Phys.* **B516** (1998) 385; *Phys. Rev.* **D63** (2001) 054510.
- [6] A. Ghinculov and Y.-P. Yao, *Mod. Phys. Lett.* **A15** (2000) 509.
- [7] A. Ghinculov and Y.-P. Yao, *Mod. Phys. Lett.* **A15** (2000) 1967; *Mod. Phys. Lett.* **A15** (2000) 925.
- [8] A. Ghinculov and J.J. van der Bij, *Nucl. Phys.* **B436** (1995) 30; A. Ghinculov, *Phys. Lett.* **B337** (1994) 137; *(E)* **B346** (1995) 426; *Nucl. Phys.* **B455** (1995) 21.
- [9] L. Durand, B.A. Kniehl and K. Riesselmann, *Phys. Rev.* **D51** (1995) 5007; *Phys. Rev. Lett.* **72** (1994) 2534; *(E)* *Phys. Rev. Lett.* **74** (1995) 1699; A. Frink, B.A. Kniehl, D. Kreimer, K. Riesselmann, *Phys. Rev.* **D54** (1996) 4548.
- [10] F.A. Berends, M. Buza, M. Böhm and R. Scharf, *Z. Phys.* **C63** (1994) 227.
- [11] R. Harlander, T. Seidensticker, M. Steinhauser, *Phys. Lett.* **B426** (1998) 125; J. Fleischer, O.V. Tarasov, F. Jegerlehner, P. Raczka, *Phys. Lett.* **B293** (1992) 437; J. Fleischer, F. Jegerlehner, M. Tentyukov, O. Veretin, *Phys. Lett.* **B459** (1999) 625.